Challenges and Implementation of Online In Situ R_{DSON} Measurement in a Three-Phase Inverter

Chondon Roy, *Member, IEEE*, Namwon Kim, *Member, IEEE*, Daniel Evans, *Member, IEEE*, James Gafford, and Babak Parkhideh, *Senior Member, IEEE*

***Abstract*—This article addresses the critical issue of real-time monitoring of ON-state resistance (R_{DSON}) of all power semiconductor devices within a three-phase inverter. An optimized ON-state voltage (V_{DSON}) measurement circuit and configuration for a multiphase converter architecture is proposed, designed to overcome the challenges posed by different characteristics and nonidealities of current and voltage sensor components. In addition to the hardware, the solution includes a data processing and qualification strategy that minimizes the impact of switching noise and processing circuitry nonidealities on R_{DSON} calculation. The efficacy of the approach is demonstrated through experimental results from a three-phase inverter, which is designed with silicon carbide metal-oxide-semiconductor field-effect transistors. This work contributes a novel solution to the field, enhancing the reliability and efficiency of power semiconductor device monitoring.**

***Index Terms*—Online in situ health monitoring, ON-state resistance (R_{DSON}).**

I. Introduction

THE widespread adoption of electric vehicles and the increasing integration of renewable energy resources are driving a growing role for power electronics in the electrical grid [1], [2]. This is further amplified by the ever-expanding volume of electronic devices in everyday applications. With such widespread adoption, a measurable subset of power electronic converters will fail in operation, resulting in cascading consequences. Among many components in the power converters, 57.1% of the converter failures are attributable to the power semiconductors [3]. As semiconductor devices are one of the primary causes of converter failures, monitoring the health status of these devices improves the overall reliability of the power converters.

In recent years, research on real-time monitoring of power electronic systems to increase reliability and prevent failure has become an important topic [4], [5], [6], [7], [8]. The power semiconductor devices (MOSFETs/IGBTs/HEMTs) age through different degradation mechanisms caused by various electro-mechanical stresses in long-term operations [9], [10], [11], [12]. Increase of ON-state resistance (R_{DSON}) results from many degradation mechanisms, such as gate-oxide degradation and bond wire degradation [13]. Therefore, R_{DSON} is a good indicator of device health status and is suitable for in situ prognostics [14], [15], [16], [17]. The power electronics community has attempted to implement in-situ monitoring of R_{DSON} of power transistors, but research has only been reported on a low-side device either in a double pulse test (DPT) setup or in a converter where the low-side device acts as an active switch such as a dc–dc boost converter or a power factor correction (PFC) converter [4], [5], [6], [7], [14], [15], [16]. Independent and simultaneous R_{DSON} measurement of individual transistors is more effective, as a failure of a single transistor may lead to the failure of the entire system. Real-time accurate R_{DSON} value of the MOSFET could be used to evaluate degradation or estimate the remaining useful lifetime [18], [19], [20], [21].

Fan et al. [22] and Mitrovic et al. [23] presented system implementation for real-time condition monitoring of MOSFETs in a three-phase inverter using R_{DSON} measurement. Fan et al. [22] present a concept of online stress index and health index generation with R_{DSON} measurement and Junction temperature estimation. Online stress and health index can be very valuable for a converter for monitoring health and predicting failure. Mitrovic et al. [23] present a concept of an integrated gate driver solution with ON-state voltage (V_{DSON}), current and dc-link voltage measurement. An integrated gate driver with health monitoring feature provides a path for scalable monitoring solutions. While both papers [22] and [23] provide R_{DSON} measurement using V_{DSON} and drain-source current (I_{DS}), there are significant differences in terms of hardware and software implementation and validation methods between our work and the previous works. Fan et al. [22] and Mitrovic et al. [23] use traditional V_{DSON} sensors referenced to the floating points of the half-bridges, making them susceptible to switching noise. Besides, both papers [22] and [23] did not provide detailed explanations on sensor synchronization and switching noise rejection methods. These are critical challenges for the implementation of the real-time in situ measurement to a practical inverter. Lack of synchronization and data qualification leads to increased probability of error in the R_{DSON} calculation specially in a high-frequency converter with high rate of change in current

Manuscript received 13 November 2023; revised 19 April 2024; accepted 27 May 2024. Date of publication 6 June 2024; date of current version 16 July 2024. This work was supported by Oak Ridge National Laboratory funded through the Department of Energy - Office of Electricity's, Transformer Resilience and Advanced Components program led by the program manager Andre Pereira. Recommended for publication by Associate Editor M. Scott. *(Corresponding author: Chondon Roy.)*

The authors are with the ECE Department, University of North Carolina at Charlotte, Charlotte, NC 28223 USA (e-mail: croy20@ford.com; kimn1@ornl.gov; daniel.evans@charlotte.edu; jgafford@charlotte.edu; bparkhideh@charlotte.edu).

Color versions of one or more figures in this article are available at https://doi.org/10.1109/TPEL.2024.3410174.

Digital Object Identifier 10.1109/TPEL.2024.3410174

TABLE I
TOTAL ISOLATED POWER SUPPLY REQUIREMENT FOR V_{DSON} SENSING

Inverter topology	Traditional V_{DSON} sensing circuit	Proposed V_{DSON} sensing circuit
3 leg, 3-phase	4	2
4 leg, 3-phase	5	2

and voltages. Papers [22] and [23] also lack proper accuracy assessments to validate their measurements, which are provided in our article.

This article presents a complete implementation of online in situ R_{DSON} monitoring of all six power transistors (MOSFETs) used in a practical three-phase DC–AC inverter containing three half-bridge (HB) legs. This article addresses the challenges of the simultaneous R_{DSON} monitoring of all MOSFETs during real-time inverter operations and proposes the implementing solution. This article offers significant improvements in accuracy and noise reduction by both hardware and software improvements. The contributions of this article are as follows.

1) A new V_{DSON} sensing circuit allowing a common reference of the analog measurement signals for all high-side MOSFETs—proposed by Roy et al. [24], [25]—is used for the online in situ R_{DSON} measurement, and its effectiveness in this application is validated for the first time. The proposed V_{DSON} sensor board reduces the complexity of power supply circuits and the size of the printed circuit board, so the board can be installed on top of the MOSFET modules seamlessly in the existing inverter hardware. This seamless integration minimizes parasitic loop resistances and impedances between MOSFET devices and the sensing circuit for more accurate R_{DSON} measurement. In addition, the drain referenced V_{DSON} sensors provide a stable reference ground for the measurement circuits making them less susceptible to switching noise. Furthermore, having a common reference for all the high side V_{DSON} sensors, our implementation reduces the total isolated power supply requirement for V_{DSON} sensing as per Table I.
2) Data sampling, synchronizing, qualifying, and computing strategies are developed to obtain meaningful R_{DSON} data out of a noisy environment during the inverter operation. The proposed signal processing strategy is essential to minimize the impact of electromagnetic interference (EMI) noises generated by sinusoidal switching operation of six MOSFET devices in a three-phase inverter. Our article presents a comprehensive algorithm for these aspects.
3) The proposed R_{DSON} monitoring system is implemented in a 75 kW three-phase inverter containing three silicon carbide (SiC) MOSFET HB modules for experimental validation. Our paper provides a comprehensive accuracy analysis and comparison with commercial measurement equipment which the existing papers lack. The true R_{DSON} of the six devices is measured under a controlled DC condition to compare with the online in situ R_{DSON} under normal AC operating conditions. A comparison of AC versus DC R_{DSON} and a comprehensive analysis of the effect of parasitic impedance is presented in this article.

The rest of this article is organized as follows. Section II presents the concept of online in situ R_{DSON} monitoring and its implementation challenges. Section III presents the complete system architecture and the V_{DSON} and current sensing circuitry. Section IV presents the proposed algorithm for data acquisition and processing on a digital microcontroller (DSP) that controls the inverter. Section V presents the hardware setup, experiment results, and a comprehensive analysis validating the proposed online in situ R_{DSON} measurement. The conclusion is presented in Section VI.

II. ONLINE IN SITU R_{DSON} MONITORING CHALLENGES AND SOLUTIONS

An online health monitoring system requires two primary components, sensors that obtain required data and a control system that processes the sensor data. The concept of online in situ R_{DSON} monitoring is to extract and record the R_{DSON} during real-time converter operation with sensors and processors within the converter. In the in situ R_{DSON} measurement, V_{DSON}, and I_{DS} measurements of power transistors need to be sent to the control system to calculate the R_{DSON}. However, in a multiphase converter with multiple HB legs, all V_{DSON} measurements of individual power transistors do not have a common V_{DSON} measurement reference with traditional sensor configuration. Therefore, the measured V_{DSON} of different devices cannot be directly tied to the control reference. This issue leads to challenges in implementing the in situ prognostics to practical power electronic converters.

For online R_{DSON} measurement in a high frequency converter very high frequency V_{DSON} and I_{DS} sensors are required. Traditional V_{DSON} sensors as described in [22], [23], [26], [27], and [28] use MOSFET's source terminals as the measurement reference. While this approach works well for low-side MOSFETs, it becomes a significant challenge for high-side devices. The source voltage of high-side MOSFETs fluctuates rapidly between the DC bus voltage and ground, with a very high rate of change (dV/dt). These voltage fluctuations make the measurement circuits susceptible to switching noise introduced through various coupling mechanisms, including capacitive, inductive, and ground loop currents. This article proposes a novel technique to address noise challenges in high-side V_{DSON} sensors by introducing a drain reference [24]. Unlike the HB midpoints, which experience significant voltage fluctuations during switching, the drain terminals of the high-side MOSFETs offer a more stable potential. By connecting the V_{DSON} sensor reference to this stable voltage source, the impact of noise injection into the measurement ground is minimized. This consequently enhances the overall noise immunity of the V_{DSON} sensor, leading to more accurate measurements.

A significant challenge in multiphase inverter design is the need for isolated power supplies for V_{DSON} sensors. Traditional methods require a separate isolated supply for each high-side V_{DSON} sensor, while low-side sensors can often share a single

supply. This approach becomes cumbersome and expensive as the number of inverter phases increases.

Our proposed drain-referenced V_{DSON} sensors for high-side MOSFETs eliminate this complexity. By utilizing the drain voltage as a reference, all high-side V_{DSON} sensors can be powered from a single isolated supply within the proposed circuit. This significantly reduces the number of isolated power supplies required. Regardless of the number of HB legs in the inverter, our approach only necessitates two isolated supplies: one for the low-side V_{DSON} sensors and one for the drain-referenced high-side V_{DSON} sensors.

In contrast, a traditional three-phase inverter with three HB legs would require one isolated supply for low-side sensors and three separate supplies for high-side sensors. Table I compares the number of isolated power supplies needed in both approaches, highlighting the cost advantage offered by our proposed solution.

When multiple switching devices are involved, their sinusoidal switching pattern generates EMI that requires special attention in analog and digital signal processing. The measured signals at different electrical nodes are affected by the EMI generated from all devices, and the measured signals contain unpredictable signal noises. Therefore, the analog data sampling strategy becomes essential to extract meaningful data from analog measurements.

This challenge has been addressed with both hardware and software implementation in this article. Our drain referenced high-side V_{DSON} sensors, significantly improve the noise immunity by providing a steady reference, similar to how the low side V_{DSON} sensors benefit from a stable reference. Furthermore, this article proposes a data synchronization and qualification algorithm that is specifically designed to ensure the accuracy of the R_{DSON} calculation under real-time inverter operation. The main considerations of the synchronization are 1) the placement of the R_{DSON} data points close to the center of the pulsewidth modulation (PWM) signal but not affecting the exiting measurements used for control and/or protection and 2) the compensation of the different voltage and current sensing delays which result in wrong R_{DSON} values. An essential layer of filtering—the data qualification—is then applied to eliminate erroneous data affected by the switching transitions of other devices under high modulation index conditions. This step is crucial for filtering out noise and ensuring the validity of the calculated R_{DSON}. Implementation details of these solutions are explained in Section IV.

Another challenge is validation of the experiment results. There are no off-the-shelf $V_{\mathrm{DSON}}/R_{\mathrm{DSON}}$ sensors readily available to compare the experiment results except with the datasheet provided numbers. The R_{DSON} provided in a standard MOSFET datasheet is a range of large number of MOSFETs. For example, the CAS300M17BM2 [29] datasheet lists 8–10 mΩ R_{DSON} for 300 A current at room temperature. It is important to know the actual R_{DSON} of the device under test (DUT) to validate the in situ measurement circuits. The maximum R_{DSON} is 25% higher than the typical value listed, which is a large number to evaluate the in situ measurement accuracy. Therefore, for an accurate comparison, each of the six MOSFETs used in the inverter are characterized under controlled preset conditions to have the baseline measurements which has been used later for comparison with the in situ measurements.

III. Proposed Solution: System Integration for Online In Situ R_{DSON} Monitoring

A. System Architecture for Online In Situ R_{DSON} Monitoring

Two measurements are required for in situ R_{DSON} measurement of a MOSFET, the $V_{\mathrm{DSON},}$ and I_{DS}. The measured signals need to be translated into the control reference to convert into digital data for further processing. The conventional voltage clamping circuit measures the V_{DSON} referenced to the source of the MOSFETs. This method allows for the same measurement reference of the V_{DSON} sensing circuits for the three low-side MOSFETs but does not provide a single measurement reference of the high-side MOSFETs. Therefore, the conventional circuit has been modified to simplify the circuit, and a new circuit is proposed to have a single measurement reference of V_{DSON} sensing circuits for the high-side MOSFETs. The R_{DSON} sensing architecture for the three-phase inverter using this new circuit for the high-side is presented in Fig. 1.

For the R_{DSON} calculation, I_{DS} is required along with the V_{DSON}. However, adding a current sensor in the switching loop on the drain or source side adds parasitic inductance, increasing loss and creating higher voltage overshoots and undershoots. Instead of adding the current sensor to the drain or source of the MOSFETs, it is connected to the outputs of the half-bridges, as presented in Fig. 1. The line current is good enough for the steady-state R_{DSON} calculation as the steady-state line current is same as the MOSFET current during the ON-state [28]. A commercial off-the-shelf current sensor [30] is used for the current measurement. Therefore, details of the current sensor are not discussed in this article.

Furthermore, the proposed architecture is minimally invasive to the existing inverter architecture. It requires electrical connections to only three outputs of the three half-bridges and the DC bus. This minimally invasive architecture can be implemented on an existing inverter setup with minimal modifications to the hardware.

B. Proposed V_{DSON} Measurement Circuit

The V_{DSON} sensing circuit solving the common signal reference issue of the high-side transistors has been designed by Roy et al. [24] and is used for the online in-situ R_{DSON} measurement for the first time in this article. The designed sensor is precise, has high voltage blocking capability and a quick dynamic response. Using the proposed V_{DSON} sensor board, all the low-side V_{DSON} sensing circuits share a common reference (DC−), and all the high-side V_{DSON} sensing circuits share another common reference (DC+). Designed high-side V_{DSON} measurement circuit, along with the low-side V_{DSON} measurement circuit, are presented in Fig. 2. Selected nodes in the circuit are marked as nodes 1, 2, 3, and 4.

The first stage blocks the high voltage when the transistor is OFF and measures only the low V_{DSON} when the transistor is

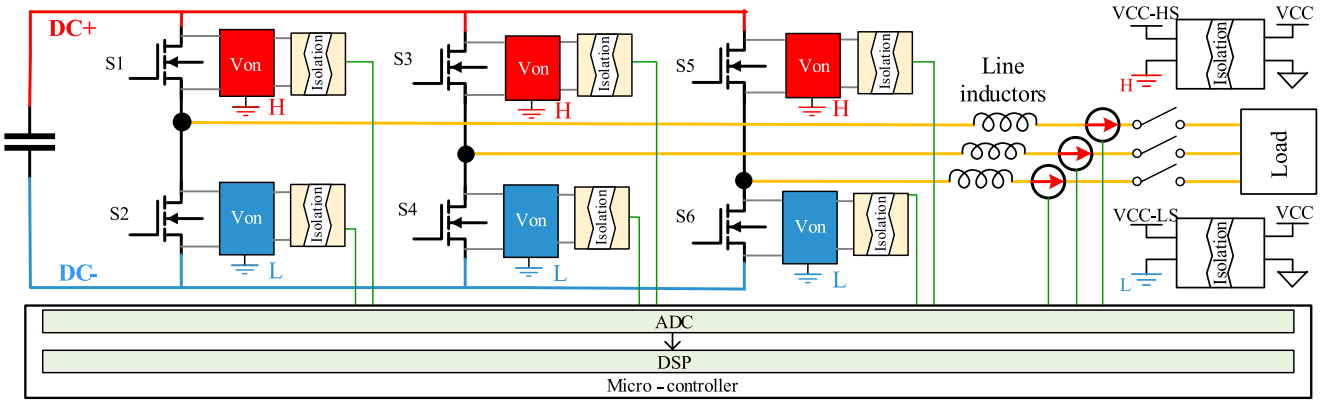

Fig. 1. In situ monitoring architecture implemented on a 3-phase inverter. *H* and *L* refers to the high-side and low-side measurement reference, respectively. VCC-HS and VCC-LS are control voltages for the high-side and low-side V_{DSON} measurement circuits respectively.

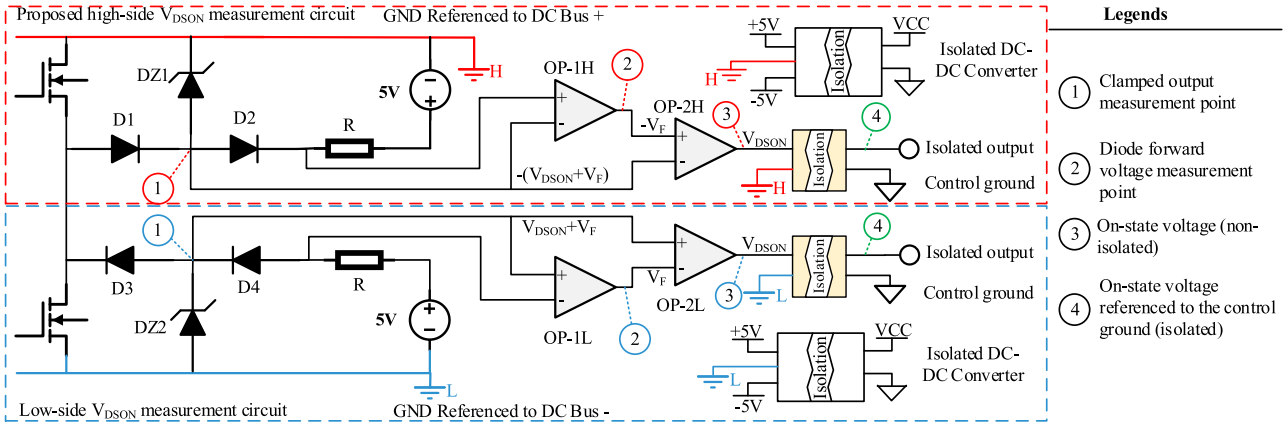

Fig. 2. Proposed circuit for high-side and low-side V_{DSON} measurement. The nodes circled red are referenced to DC+, the nodes circled blue are referenced to DC- and the nodes circled green are referenced to the control ground. Same circuit is repeated for the three-phases except the same power supplies are used for all three-phases.

ON. A high voltage (1.2 kV) Schottky blocking diode (D1) [31] is connected to the source of the high-side transistor, which only allows current flow from the source to the V_{DSON} measurement circuit. When the transistor is turned OFF, D1 becomes reverse biased and disconnects the source terminal from the measurement circuit. A Zener diode DZ1 is used between measurement node1 and the corresponding ground to set the OFF-state voltage at node1. This ensures node1 maintaining a specific voltage regardless of fluctuations in the auxiliary power supply voltage. Additionally, the Zener diode provides a freewheeling path for the current within the clamping circuit during the OFF-state. This freewheeling path is crucial because without it, a high voltage overshoot would occur at node1 when the blocking diode (D1) transitions from forward bias to reverse bias. When the transistor is turned ON, D1 becomes forward biased, completing the circuit through the transistor. During the ON-state, node 1 measures the inverted sum of V_{DSON} and the forward voltage drop (V_F) of D1, which is - *(V_{DSON} + V_F)*. Actual V_{DSON} can be calculated by subtracting V_F from the absolute value of the voltage at node 1. A second Schottky diode (D2), identical to D1, is placed in series very close to D1 so that they operate at a similar temperature level [27]. When the DUT is ON, the same current flows through these two diodes (D1 and D2), ensuring the same forward voltage drop. The voltage drop across the second diode (D2) is measured using a differential amplifier circuit [32] which is a part of the second stage of the V_{DSON} measurement circuit. The output of this circuit is measured at node 2. The voltage at node 1 is then subtracted from the voltage at node 2, to get the V_{DSON} of the DUT, which is indicated at node 3. Node 4 is the output of the last stage that isolates the measured V_{DSON} from the measurement circuit reference (DC+) to the control circuit reference. This is implemented using an off-the-shelf analog isolation amplifier (ADuM4190) [33].

The low-side V_{DSON} measurement circuit works in a similar way, except it references the negative DC bus (DC−). The voltages at different measurement nodes depending on the status of the particular MOSFET are summarized in Table II. Further details of the sensing circuit such as design details and output performance are presented in [24].

IV. Proposed Solution: Online In Situ R_{DSON} Calculation and Reporting

The V_{DSON} and I_{DS} sensor outputs are sampled and processed through a DSP for the real-time R_{DSON} update feature. The sampled data go through a series of data qualification stages to achieve accurate and meaningful measurements.

TABLE II
V_{DSON} CIRCUIT OPERATION AND MEASUREMENTS AT DIFFERENT NODES

Node	MOSFET status	High-side	Low-side
1	ON	$-(V_{DSON}+V_F)$	$V_{DSON}+V_F$
	OFF	−3 V	3 V
2	X	$-V_F$	V_F
3	ON	$V_{DSON}=V_{NODE2}-V_{NODE1}$	$V_{DSON}=V_{NODE2}-V_{NODE1}$
	OFF	$3-V_F=V_{NODE2}-V_{NODE1}$	$3-V_F=V_{NODE2}-V_{NODE1}$

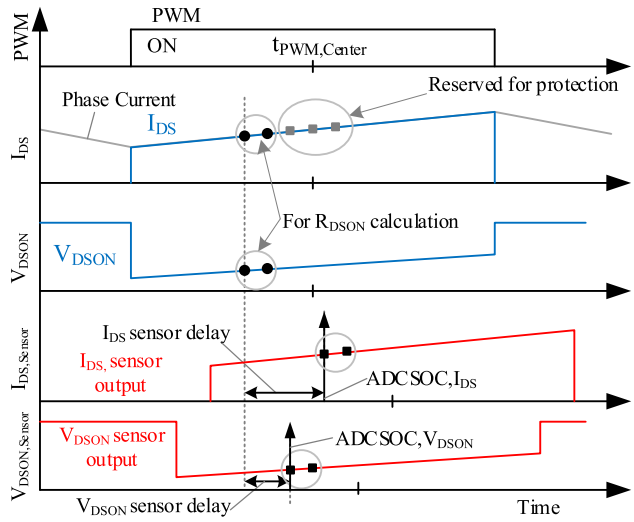

Fig. 3. V_{DSON} and I_{DS} sampling synchronization for instantaneous R_{DSON} calculation. Blue lines indicate the ideal current and voltage waveforms, and the red lines represent the measured signals. The measurement delay is characterized to align the current and voltage measurements.

A. Data Sampling and Synchronization for Online R_{DSON} Calculation

The first step is reading the V_{DSON} and I_{DS} sensor outputs using the analog-to-digital converter (ADC) module in a DSP. Synchronization of ADC sampling with the PWM signal is one of the important implementation considerations. As shown in Fig. 3, the effective V_{DSON} and I_{DS} waveforms (blue lines) appear when the device is on. Hence, the ADC sampling needs to be completed within this short period. In particular, the center of the PWM on time ($t_{PWM,Center}$) is the preferred area for accurate ADC sampling by avoiding the potential signal noise near the PWM switching transitions. In fact, three AC inductor currents (I_{La}, I_{Lb}, I_{Lc}) used for the primary inverter functions such as closed-loop control and protection are already sampled at $t_{PWM,Center}$. Two additional samples of each V_{DSON} and I_{DS} for the online R_{DSON} calculation are captured in advance to the three AC inductor current measurements so that the implementation of the R_{DSON} measurement does not affect the performance of the exiting primary inverter functions. These V_{DSON} and I_{DS} measurements are captured before the three AC inductor current samples, as shown in Fig 3. ADC start-of-conversion (SOC) triggers, ADCSOC,I_{DS} and ADCSOC,V_{DSON}, are programmed to start sampling V_{DSON} and I_{DS}. The V_{DSON} and I_{DS} sensing

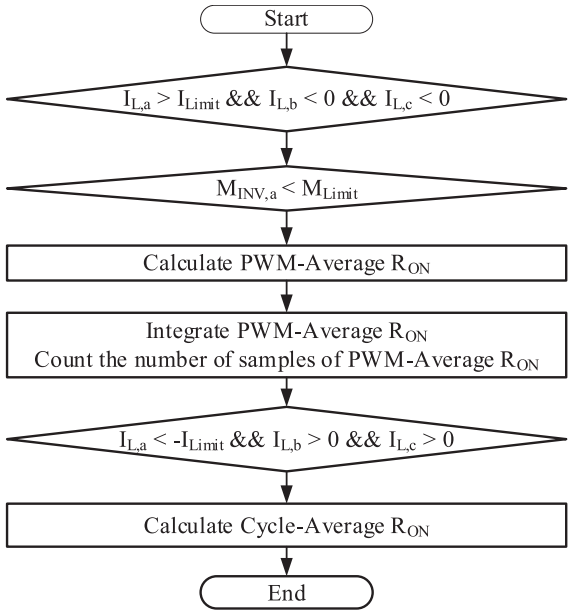

Fig. 4. Developed flowchart for R_{DSON} calculation: Example is shown only for one device, the phase A high-side MOSFET. This is repeated sequentially to get R_{DSON} of all six MOSFETs in one AC-cycle.

circuits have different signal output delays, as shown in Fig. 3 (red lines). These delays are characterized through experiments and presented in the next section. To compensate for these sensing delays, the two ADCSOC triggers are shifted independently to synchronize the V_{DSON} and I_{DS} measurements. As the ADCSOC trigger sources, two unused ePWM channels of the DSP are used, and their event trigger timings are adjusted to apply the different sensor output delays to the ADC sampling as illustrated as the vertical arrows in the fourth and fifth rows in Fig. 3.

B. Data Qualification to Filter Noisy Data From Calculation

Due to practical issues of hardware circuit components, false or noisy sensing output signals may inadvertently be applied to the microcontroller. The first challenge is that the isolated analog amplifier, ADuM4190 [33], has a lower common-mode input range, which does not provide accurate isolated output for inputs that is less than 200 mV. To address this limitation, R_{DSON} is only calculated above 30 A phase current of the inverter. 30 A phase current corresponds to 210 mV voltage drop across the drain and source terminal of the MOSFET considering 7 mΩ R_{DSON}. In addition, switching transitions of other phases cause EMI noise on the V_{DSON} and I_{DS} sensing signals, even though the ADC readings are synchronized near the $t_{PWM,Center}$. It is confirmed that a switching event when the modulation index (of the phase being sampled) is less than 0.85 provides enough time to avoid the switching noise interference from other phases and have noise-free ADC samples. Therefore, the effective range of the modulation index for the R_{DSON} measurement is limited to less than 0.85. The data qualification flow chart is shown in Fig. 4.

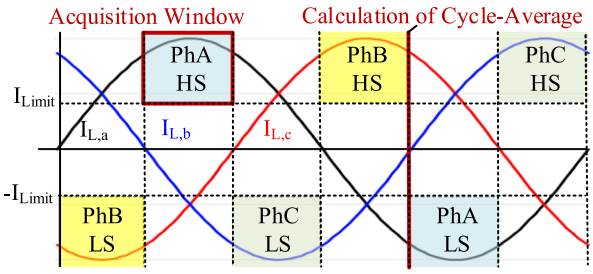

Fig. 5. Three-phase current and voltage sampling window. Shaded areas indicate the current and voltage data acquisition window for the six MOSFETs. Average is calculated in the beginning of the data acquisition of the complementary device of the same leg.

TABLE III
SPECIFICATION OF THE 3-PHASE INVERTER

Parameter	Value
Maximum rated power	75 kW
Nominal input voltage	1000 VDC
Output voltage	480 VAC
Switching frequency	30 kHz
SiC module	CAS300M17BM2

C. Average R_{DSON} Calculation and Reporting

When calculating R_{DSON}, multiple samples of R_{DSON} values are averaged to minimize random fluctuations of the measured data. The PWM-average R_{DSON} is calculated by averaging two samples of R_{DSON} data obtained within a single PWM cycle. The PWM-average R_{DSON} values are integrated during the acquisition window shown in Fig. 5, and the R_{DSON} sum is divided by the number of PWM cycles counted during the acquisition window. The resulted value of this averaging process is called cycle-average R_{DSON}. The cycle-average R_{DSON} is obtained at the beginning of the acquisition window of the opposite device in the same phase leg. This calculation timing is designed to cope with the variation in the width of the acquisition window, which varies according to the inverter's operating condition. All six cycle average R_{DSON} data are updated every fundamental frequency cycle.

V. Hardware Setup and Experiment Results

The in situ R_{DSON} monitoring is implemented on a 75 kW three-phase inverter. The specification of the inverter is presented in Table III. The inverter consists of different boards assembled together, as per the cross section shown in Fig. 6. The V_{DSON} sensing board is mounted directly on top of the SiC HB modules. The line current sensors are mounted around the bushing terminals of the output terminals of the inverter. The motherboard has a TI DSP F28379D controlCARD for inverter control and R_{DSON} calculation. Fig. 7 presents a photograph of the developed inverter, which includes the power stage and additional auxiliary components.

R_{DSON} is calculated in three different experiments, 1) DPT; 2) DC condition; and 3) sinusoidal inverter operation.

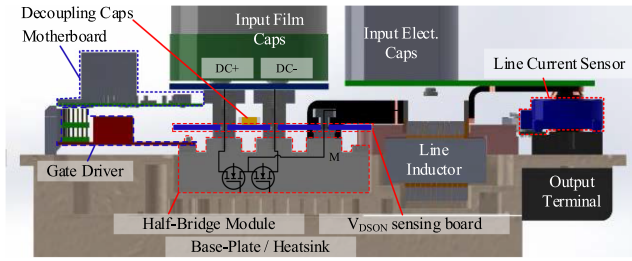

Fig. 6. Cross section of the inverter power stage.

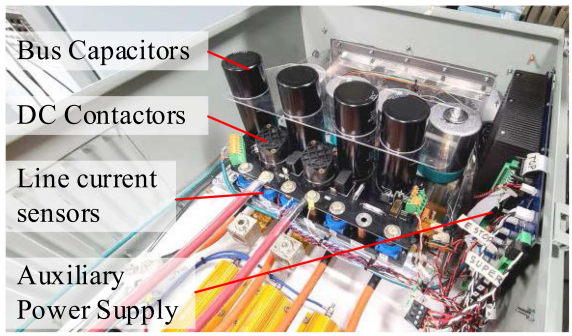

Fig. 7. Developed inverter assembly, includes the power stage, auxiliary power unit, precharge circuitry, contactors, and cooling fans.

A. Sensor Dynamic Characterization in DPT

To find the V_{DSON} and I_{DS} sensor output dynamic characteristics, a DPT is conducted. It has been found that the analog isolator adds 1.2 μs time delay in the measured signal of the V_{DSON} sensor. Similarly, the hall effect current sensor adds 3 μs delay to the measured signal compared to the actual current. The current sensor measurement is compared with a Tektronix current probe (TCP0150), having less than 40 ns delays. Fig. 8 presents the delays of the V_{DSON} and I_{DS} sensor outputs. These delays are compensated for, later, during analog data sampling for the R_{DSON} calculation.

B. True R_{DSON} Reference Generation Under DC

The actual DC R_{DSON} of the three modules used in the inverter is measured using precision digital multimeters (DMMs). It is a necessary process to obtain the true R_{DSON} data of the specific SiC MOSFET devices we used to validate the online in situ R_{DSON} measurement results.

The circuit diagram of the experiment setup and the measured R_{DSON} are presented in Fig. 9. A current source is connected to the DUT with a series-connected precision shunt resistor. The voltage across the DUT and the shunt are measured using DMMs. Then the R_{DSON} is calculated using the DMM measurements. The R_{DSON} of the six MOSFETs at 40 A current is listed in Table IV. The R_{DSON} of the six MOSFETs are 6.6, 6.4, 5.9, 5.8, 6.4, and 6.4 mΩ for S1, S2, S3, S4, S5, and S6, respectively, at 40 A current, which is the selected current for the AC operation.

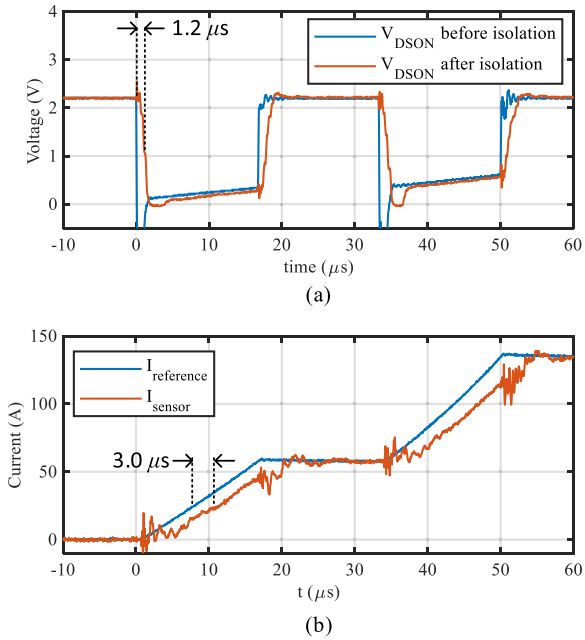

Fig. 8. Experimental evaluation of the voltage and current sensing delays. Isolated V_{DSON} sensor output and current sensor output have 1.2 and 3.0 μs delay, respectively. (a) V_{DSON} sensing delay, and (b) Current sensing delay.

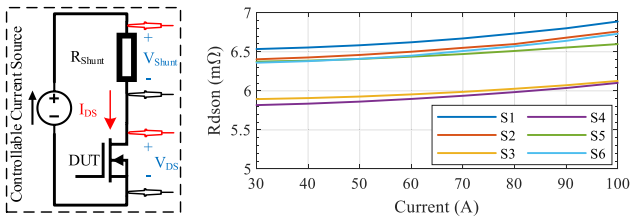

Fig. 9. True R_{DSON} measurement for reference point generation: True (DC) R_{DSON} of the three SiC modules used in the inverter using DMM. Schematic of the test setup (left) and the results (right). The true R_{DSON} data is used to compare with the online measurements.

TABLE IV
TRUE (DC) R_{DSON} OF THE SIX MOSFETS AT 40 A CURRENT (EXPERIMENTAL RESULTS FOR REFERENCE POINTS GENERATION)

Device	S1	S2	S3	S4	S5	S6
$R_{DSON}(m\Omega)$	6.6	6.4	5.9	5.8	6.4	6.4

C. Online In Situ R_{DSON} Measurement in Sinusoidal Inverter Operation

For regular inverter operation, all six MOSFETs turn ON and OFF simultaneously following the sinusoidal PWM to generate sinusoidal three-phase output. Fig. 10(a) presents the oscilloscope capture of the V_{DSON} and phase current waveforms in phase-A. The V_{DSON} of the high-side MOSFET is proportional to the positive half cycle of the phase current, and the V_{DSON} of the low-side MOSFET is proportional to the negative half cycle of the phase current. Fig. 10(b) presents the sampled V_{DSON} and I_{DS} data points of the Phase-A high-side MOSFET per every switching cycle during the half cycle of the AC output. These

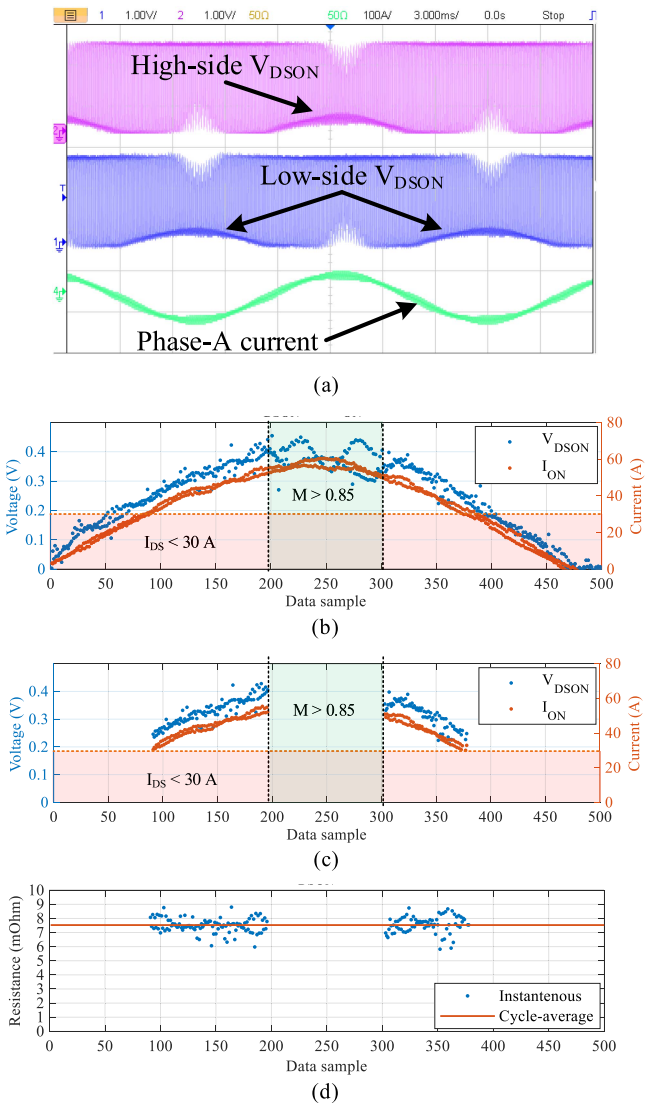

Fig. 10. Experimental results under 1000 V DC–480V AC: Phase A V_{DSON} measurement experimental results for half grid cycle. (a) Oscilloscope capture, (b) sampled V_{DSON} and I_{DS} in the DSP, (c) samples after the data qualifications, and (d) calculated instantaneous and average R_{DSON}.

data points are recorded on the DSP memory and extracted for validation. At the center of the half cycle, where the modulation index is higher than 0.85, the switching noise interferences are observed and are discarded as per the data qualification algorithm. Fig. 10(c) shows data points after the data qualification. After that, PWM-average and cycle-average R_{DSON} values are calculated, as shown in Fig. 10(d). These results verify the feasibility and the effectiveness of the proposed in situ R_{DSON} measurement system architecture and data processing.

For online health monitoring, the cycle averaged R_{DSON} data are recorded and saved. As R_{DSON} is expected to change slowly over a long operating lifetime, the cycle-average R_{DSON} is further averaged every second to reduce the memory requirement to store and process a large number of R_{DSON} data. Fig. 11 presents recorded averaged R_{DSON} for 300 s. The averages of these 300 s data points are 7.5, 6.8, 6.4, 6.0, 6.9, and 6.9 mΩ for S1, S2, S3,

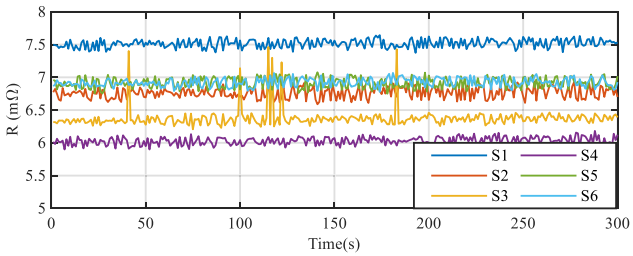

Fig. 11. Experimental results: In situ R_{DSON} measurement over 300 s (averaged every 1 s) under 1000 V DC–480 V AC at 30 kW.

TABLE V
ONLINE AC R_{DSON} OF THE SIX MOSFETS AND TRUE (DC) R_{DSON} UNDER SAME OPERATING CONDITIONS

Device No	S1	S2	S3	S4	S5	S6
True (DC) R_{DSON} @40A (mΩ)	6.6	6.4	5.9	5.8	6.4	6.4
AC-Online In-situ R_{DSON} @40A (mΩ)	7.5	6.8	6.4	6.0	6.9	6.9
Difference btw DC and Online R_{DSON} @40A (mΩ)	0.9	0.4	0.5	0.2	0.5	0.5

S4, S5, and S6, respectively. The R_{DSON} of S3 has some random spikes up to 1 mΩ above the average value. A possible reason for the spikes could be noise source along the propagation path of the $V_{\mathrm{DSON}}/I_{\mathrm{DS}}$ sensing signal for this MOSFET. Regardless of the spikes, the data are consistent most of the time. Comprehensive analysis of the measured online R_{DSON} is presented in the next section.

D. AC Impedance Analysis

To find the efficacy of the proposed online in situ R_{DSON} monitoring architecture the true R_{DSON} of each of the six MOSFETs have been characterized under DC conditions to find the baseline R_{DSON}. The details of the DC characterization test are presented in Section V-B. These R_{DSON} references are the true R_{DSON} of the six MOSFETs as these were measured using precision digital multimeters in a controlled condition.

The true (DC) and online in situ R_{DSON} values at 40 A current are picked from Figs. 9 and 11 and listed in Table V. The online in situ impedances at 40 A current are measured between 6 and 7.5 mΩ. The average online R_{DSON} of the six MOSFETs at 40 A is found to be 6.8 mΩ, where the average dc R_{DSON} at the same condition from Fig. 9 is 6.3 mΩ. In average, the online R_{DSON} is 0.5 mΩ higher than the DC measurements. This deviation between the DC and online measurement should not be considered as a measurement error but effect of the parasitic impedances during AC operation. The online measurement includes parasitic elements that increase the impedance as frequency increases. The impedance seen from the sensor connection point is presented in Fig. 12. Therefore, the measured impedance can be expressed as follows:

$$Z_{\mathrm{Meas}} = R_{\mathrm{DS}} \,||\, \left(\frac{1}{j\omega C_O}\right) + j\omega L_{\mathrm{stray}} + R_{\mathrm{contact}} \qquad (1)$$

where $Z_{\mathrm{Meas}}$is the measured impedance, $1/j\omega C_o$ is impedance due to the output capacitance of the DUT, $j\omega L_{\mathrm{stray}}$ is the impedance due to the stray inductance, and R_{contact} is the contact resistance between the V_{DSON} sensor board and HB module, and ω is the frequency of operation. The typical values C_O and L_{stray} are given as 2.9 nF and 15 nH for the SiC module (CAS300M17BM2) tested [29]. As an example, if the resistance for DC R_{DSON} is 6.2 mΩ and the contact resistance is 0.1 mΩ, these values will produce an impedance of

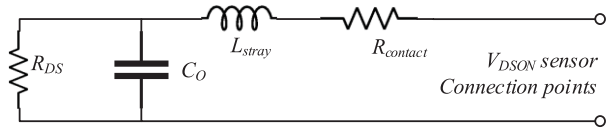

Fig. 12. Representation of the electrical parasitic elements between the MOSFET and V_{DSON} sensor interconnection.

$$Z_{\mathrm{Meas}} = 0.0062 || \left(\frac{1}{j\omega \times 2.9 \times 10^{-9}}\right) + j\omega \times 15 \times 10^{-9} + 0.0001 \qquad (2)$$

which results in $Z = 6.905\ \mathrm{m\Omega}$ at 30 kHz, and $Z = 6.3\ \mathrm{m\Omega}$ at DC. Therefore, an increase of $0.605\ \mathrm{m\Omega}$ R_{DSON} is expected under AC condition running at 30 kHz compared to the DC measurements. This increase in the magnitude of impedance, $0.605\ \mathrm{m\Omega}$ in this theoretical example based on the datasheet, is in the same range as the measured $0.5\ \mathrm{m\Omega}$ average increase of the online in situ R_{DSON} under sinusoidal AC condition compared to the true (DC) R_{DSON}. The difference between the DC R_{DSON} and the in situ R_{DSON} for the six MOSFETs is presented in Table IV.

VI. CONCLUSION

A complete architecture for an online in situ R_{DSON} monitoring has been presented in this article. Various design challenges, such as propagation delays, switching noises, and the operating range of isolators, have been meticulously addressed. A new V_{DSON} sensing circuitry, developed with a focus on reducing component count, has been innovatively designed to effectively capture the on-state voltages of high-side and low-side switches of a practical inverter. A software algorithm has been proposed and implemented that collects real-time V_{DSON} and I_{DS} data, filters useful data, calculates and reports the in situ R_{DSON} of the power MOSFETs. Real-time R_{DSON} of the six MOSFETs under 1000 VDC to 480 VAC sinusoidal operation at 30 kW power have been presented in this article demonstrating the effectiveness of our approach. It was observed that the online in situ AC R_{DSON} of the six MOSFETs ranges 6.0 to 7.5 mΩ which is on average 0.5 mΩ higher than the DC (true) R_{DSON}. This increase is attributed to the parasitic impedances that only affect the AC measurements. A comprehensive AC impedance analysis has been presented that supports these observations. The insights gained from this study can be instrumental in assessing the degradation and predicting the remaining useful lifetime of the inverter. While our findings are promising, it is acknowledged that further research is needed to refine our approach and expand

its applicability. This work marks a significant step forward in the field of online health monitoring of power electronics and opens up new avenues for future research.

REFERENCES

[1] B. K. Bose, "Global energy scenario and impact of power electronics in 21st century," *IEEE Trans. Ind. Electron.*, vol. 60, no. 7, pp. 2638–2651, Jul. 2013.

[2] Yole Group, "Power electronics, A green revolution is giving way to new power electronics applications," Accessed: Apr. 17, 2024, [Online]. Available: https://www.yolegroup.com/thematic/power-electronics-application/

[3] L. F. Costa and M. Liserre, "Failure analysis of the dc-dc converter: A comprehensive survey of faults and solutions for improving reliability," *IEEE Power Electron. Mag.*, vol. 5, no. 4, pp. 42–51, Dec. 2018.

[4] J. Morroni, A. Dolgov, M. Shirazi, R. Zane, and D. Maksimovic, "Online health monitoring in digitally controlled power converters," in *Proc. IEEE Power Electron. Spec. Conf.*, 2007, pp. 112–118.

[5] S. Pu, F. Yang, B. T. Vankayalapati, E. Ugur, C. Xu, and B. Akin, "A practical on-board SiC MOSFET condition monitoring technique for aging detection," *IEEE Trans. Ind. Appl.*, vol. 56, no. 3, pp. 2828–2839, May/Jun. 2020.

[6] F. Gonzalez-Hernando, J. San-Sebastian, M. Arias, A. Rujas, and F. Iannuzzo, "Discontinuous PWM for online condition monitoring of SiC power modules," *IEEE J. Emerg. Sel. Topics Power Electron.*, vol. 8, no. 1, pp. 323–330, Mar. 2020.

[7] H. You et al., "Intelligent health monitoring system hardware design for paralleled devices with fast dv/dt output," in *Proc. IEEE Int. Elect. Mach. Drives Conf.*, 2021, pp. 1–5.

[8] E. Ugur, C. Xu, F. Yang, S. Pu, and B. Akin, "A new complete condition monitoring method for SiC power MOSFETs," *IEEE Trans. Ind. Electron.*, vol. 68, no. 2, pp. 1654–1664, Feb. 2021.

[9] J. Millán, P. Godignon, X. Perpiñà, A. Pérez-Tomás, and J. Rebollo, "A survey of wide bandgap power semiconductor devices," *IEEE Trans. Power Electron.*, vol. 29, no. 5, pp. 2155–2163, May 2014.

[10] A. J. Lelis, R. Green, and D. B. Habersat, "SiC MOSFET reliability and implications for qualification testing," in *Proc. IEEE Int. Rel. Phys. Symp.*, 2017, pp. 2A–4.1–2A–4.4.

[11] J. Wei, S. Liu, J. Fang, S. Li, T. Li, and W. Sun, "Investigation on degradation mechanism and optimization for SiC power MOSFETs under long-term short-circuit stress," in *Proc. IEEE 30th Int. Symp. Power Semicond. Devices ICs*, 2018, pp. 399–402.

[12] X. Yang et al., "Degradation behavior and defect analysis for SiC power MOSFETs based on low-frequency noise under repetitive power-cycling stress," *IEEE Trans. Electron Devices*, vol. 68, no. 2, pp. 666–671, Feb. 2021.

[13] E. Ugur, F. Yang, S. Pu, S. Zhao, and B. Akin, "Degradation assessment and precursor identification for SiC MOSFETs under high temp cycling," *IEEE Trans. Ind. Appl.*, vol. 55, no. 3, pp. 2858–2867, May/Jun. 2019.

[14] R. Li, X. Wu, S. Yang, and K. Sheng, "Dynamic on-state resistance test and evaluation of GaN power devices under hard- and soft-switching conditions by double and multiple pulses," *IEEE Trans. Power Electron.*, vol. 34, no. 2, pp. 1044–1053, Feb. 2019.

[15] S. Dusmez, M. Bhardwaj, L. Sun, and B. Akin, "In situ condition monitoring of high-voltage discrete power MOSFET in boost converter through software frequency response analysis," *IEEE Trans. Ind. Electron.*, vol. 63, no. 12, pp. 7693–7702, Dec. 2016.

[16] J. Chen, X. Jiang, Z. Li, H. Yu, and J. Wang, "Investigation on degradation of SiC MOSFET under accelerated stress in PFC converter," in *Proc. IEEE Energy Convers. Congr. Expo.*, 2019, pp. 6174–6178.

[17] Y. Peng, Y. Shen, and H. Wang, "A condition monitoring method for three phase inverter based on system-level signal," in *Proc. IEEE Int. Power Electron. Application Conf. Expo.*, 2018, pp. 1–5.

[18] M. Biglarbegian et al., "On condition monitoring of high frequency power GaN converters with adaptive prognostics," in *Proc. IEEE Appl. Power Electron. Conf. Expo.*, 2018, pp. 1272–1279.

[19] S. Dusmez, H. Duran, and B. Akin, "Remaining useful lifetime estimation for thermally stressed power MOSFETs based on on-State resistance variation," *IEEE Trans. Ind. Appl.*, vol. 52, no. 3, pp. 2554–2563, May/Jun. 2016.

[20] Y. Chen and D. B. Ma, "Self-Aging-prognostic GaN-based switching power converter using TJ-independent online condition monitoring and proactive temperature frequency scaling," *IEEE Trans. Power Electron.*, vol. 36, no. 5, pp. 5022–5031, May 2021.

[21] M. Baharani, M. Biglarbegian, B. Parkhideh, and H. Tabkhi, "Real-time deep learning at the edge for scalable reliability modeling of Si-MOSFET power electronics converters," *IEEE Internet Things J.*, vol. 6, no. 5, pp. 7375–7385, Oct. 2019.

[22] J. Fan, D. Ma, J. Wang, M. Chinthavali, and RSK. Moorthy, "Real-time condition monitoring of power modules in grid-tied power converter," in *Proc. IEEE Energy Convers. Congr. Expo.*, 2022, pp. 1–6.

[23] V. Mitrovic, B. Fan, Y. Cao, Y. Bai, R. Burgos, and D. Boroyevich, "Phase current reconstruction, DC link voltage and R DS-ON measurement using sensors integrated on gate drivers for SiC MOSFET," in *Proc. 22nd Int. Symp. Power Electron.*, 2023, vol. 1, pp. 1–6.

[24] C. Roy, N. Kim, J. Gafford, and B. Parkhideh, "On-state voltage measurement of high-side power transistors in three-phase four-leg inverter for in-situ prognostics," in *Proc. IEEE Energy Convers. Congr. Expo.*, 2021, pp. 2770–2776.

[25] C. Roy, "In-situ instrumentation for degradation monitoring of power semiconductor devices in power electronics converters," Ph.D. dissertation, Univ. North Carolina Charlotte, Charlotte, NC, USA, 2023.

[26] N. Badawi and S. Dieckerhoff, "A new method for dynamic ron extraction of GaN power HEMTs," in *Proc. Int. Exhib. Conf. Power Electron., Intell. Motion, Renewable Energy Manage.*, 2015, pp. 1–6.

[27] M. Guacci, D. Bortis, and J. W. Kolar, "On-state voltage measurement of fast switching power semiconductors," *CPSS Tran. Power Electron. Appl.*, vol. 3, no. 2, pp. 163–176, Jun. 2018.

[28] C. Roy and B. Parkhideh, "Design consideration for characterization and study of dynamic on state resistance of GaN devices," in *Proc. IEEE 7th Workshop Wide Bandgap Power Dvices Appl.*, 2019, pp. 181–186.

[29] Cree Inc., Durham, NC, USA, "1.7kV, 8.0 mΩ all-silicon carbide half-bridge module," CAS300M17BM2 datasheet, Jan. 2020.

[30] LEM USA Inc., Meyrin, Switzerland, "Current transducer HTFS 200 … 800-P," HTFS 200-P datasheet, Nov. 2022.

[31] GeneSiC Semiconductor, Torrance, CA, USA, "1200V 2A SiC Schottky MPSTM diode," GB02SLT12-214 datasheet, Nov. 2022.

[32] J. Bird, *Electrical Circuit Theory and Technology*, 4th ed. Amsterdam, The Netherlands: Newnes/Elsevier, 2010, pp. 253–254.

[33] Analog Devices, Wilmington, CA, USA, "High stability isolated error amplifier," ADuM4190 datasheet, Mar. 2022.

Chondon Roy (Member, IEEE) received the B.Sc. degree in electrical and electronic engineering from Bangladesh University of Engineering and Technology, Dhaka, Bangladesh, in 2017, and the Ph.D. degree in Electrical Engineering from University of North Carolina at Charlotte, NC, USA, in 2023. He is currently a core power electronics engineer in the electric vehicle division at Ford Motor Company. He specializes in power electronics solutions for EV and has a keen interest in the design and control of Power Electronics systems, reliability assessment of WBG devices, and sensor design for online in-situ condition monitoring of Power converters.

Namwon Kim (Member, IEEE) received the B.S. and M.S. degrees in electrical engineering from Changwon National University, Changwon, South Korea, in 2010 and 2012, respectively, and the Ph.D. degree in electrical engineering from the University of North Carolina at Charlotte, Charlotte, NC, USA, in 2022. He is currently an R&D Associate at Oak Ridge National Laboratory. His research interests include design and control of power electronic converters in the applications of renewable energy, energy storage, and EV chargers.

Daniel Evans (Member, IEEE) received the B.S. degree in computer engineering, and the M.S. and Ph.D. degrees in electrical engineering from the University of North Carolina at Charlotte, Charlotte, NC, USA, in 2009, 2013, and 2018, respectfully. He is currently with the Energy Production and Infrastructure Center (EPIC) at the University of North Carolina at Charlotte as a Power Electronics Research Engineer. His current research is focused on sensor integration for advanced prognostics and protection in power converters, centralized and distributed controls, emerging energy storage solutions, and embedded solutions for control loop and DSP processing in power converters.

James Gafford received the bachelor's degree from Christian Brothers University, Memphis, TN, USA, in 1999, and the master's degree from Mississippi State University, Mississippi State, MS, USA, in 2005, both in electrical engineering. He is currently working as the Assistant Director of Research and Special Projects with the Energy Production and Infrastructure Center. Mr. Gafford has more than 15 years of experience in university research and development laboratories. His previous work includes the development of advanced power electronics and vehicle autonomy.

Babak Parkhideh (Senior Member, IEEE) received the B.Sc. degree with honors from the University of Tehran, Tehran, Iran, in 2003, the M.Sc. degree from RWTH-Aachen University, Aachen, Germany, in 2006, and the Ph.D. degree from North Carolina State University, Raleigh, NC, USA, in 2012, all in electrical engineering. He is an Associate Professor in the Department of Electrical and Computer Engineering, University of North Carolina at Charlotte, Charlotte, NC, USA, where he is also a Faculty Associate with the Energy Production and Infrastructure Center (EPIC) and the founding director of the PV Integration Laboratory (PIL). Dr. Parkhideh has published over 100 papers in journals and conference proceedings His recent research interests include PV/battery power electronic systems, control and prognostics of high-frequency power converters, and high-bandwidth sensing schemes.